scientific reports

Check for updates

OPEN

Adaptations of endolithic communities to abrupt environmental changes in a hyper-arid desert

Cesar A. Perez-Fernandez[1], Paul Wilburn[2], Alfonso Davila[2] & Jocelyne DiRuggiero[1,3]✉

The adaptation mechanisms of microbial communities to natural perturbations remain unexplored, particularly in extreme environments. The extremophilic communities of halite (NaCl) nodules from the hyper-arid core of the Atacama Desert are self-sustained and represent a unique opportunity to study functional adaptations and community dynamics with changing environmental conditions. We transplanted halite nodules to different sites in the desert and investigated how their taxonomic, cellular, and biochemical changes correlated with water availability, using environmental data modeling and metagenomic analyses. Salt-in strategists, mainly represented by haloarchaea, significantly increased in relative abundance at sites characterized by extreme dryness, multiple wet/dry cycles, and colder conditions. The functional analysis of metagenome-assembled genomes (MAGs) revealed site-specific enrichments in archaeal MAGs encoding for the uptake of various compatible solutes and for glycerol utilization. These findings suggest that opportunistic salt-in strategists took over the halite communities at the driest sites. They most likely benefited from compounds newly released in the environment by the death of microorganisms least adapted to the new conditions. The observed changes were consistent with the need to maximize cellular bioenergetics when confronted with lower water availability and higher salinity, providing valuable information on microbial community adaptations and resilience to climate change.

Desert microbial communities are dominated by organisms that can survive desiccation and quickly resume growth after a wetting event. The dependence on stochastic and meager inputs of liquid water exerts a marked control on how desert organisms assemble and the types of substrates they colonize. In semi-arid and arid regions, biological soil crusts (BSCs) form a thin veneer of biological activity on the top few centimeters of soils[1]. With increasing dryness, BSCs become fragmented and patchy[1], and many microorganisms find refuge on the underside of translucent rocks such as quartz (e.g. hypolithic communities). In hyper-arid regions, hypolithic communities are replaced by endolithic communities colonizing the interior spaces of rocks[2,3].

The hyper-arid core of the Atacama Desert in northern Chile is one of the driest regions on Earth. Primary productivity almost exclusively occurs inside halite (NaCl) nodules found on the surface of evaporitic playas (called salares)[4–7]. The communities inhabiting these nodules are composed of archaea, with *Halobacteria* constituting most of the biomass, unique *Cyanobacteria*, diverse heterotrophic bacteria, and a single species of halophilic alga (*Dolichomastix*)[4–6]. The primary sources of liquid water for these communities are fog, dew, and salt deliquescence[8]. Far from representing an ecological curiosity of little significance, the Atacama halite communities are a unique example of taxonomic and functional adaptability to poly-extreme conditions of temperature, water availability, salinity, and radiation[4,9,10].

The study of these communities can reveal new clues about the factors that control growth, taxonomic diversity, and physiological function near the dry limit of habitability. For example, the carbon isotopic composition (^{13}C and ^{14}C) of phospholipid fatty acids in colonized halite nodules indicates modern carbon fixation and community turnover rates of several years. However, the presence of radiocarbon enriched fatty acids also points to a significant amount of carbon recycling within the community[11]. In contrast, turnover rates in other lithic communities in hyper-arid settings, notably colder ones, are likely decades to hundreds of years or longer (e.g., Colesie et al.[12]; Mergelov et al.[13]). In addition, archaea comprise a significant fraction of halite communities[4,14],

[1]Department of Biology, The Johns Hopkins University, Baltimore, MD, USA. [2]NASA Ames Research Center-Exobiology Branch MS 239-4, Moffett Field, CA, USA. [3]Department of Earth and Planetary Sciences, The Johns Hopkins University, Baltimore, MD, USA. ✉email: jdiruggiero@jhu.edu

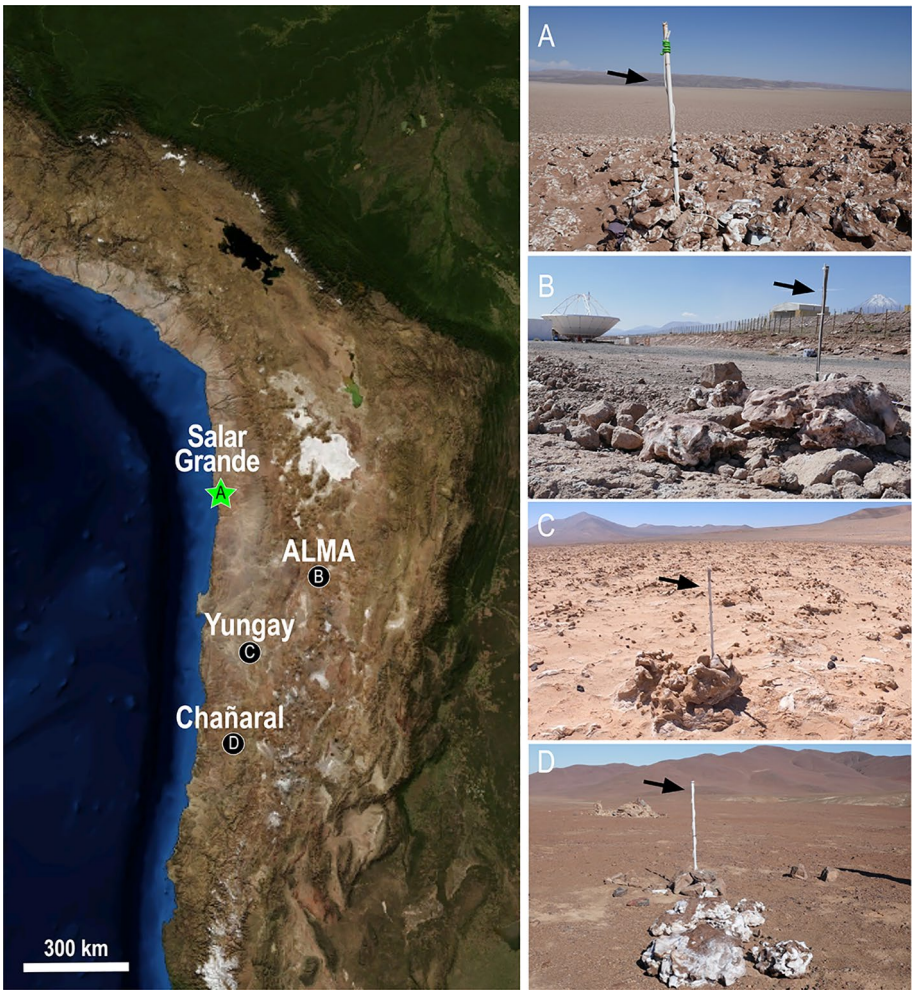

Figure 1. *Left* Satellite image of part of the Atacama Desert in northern Chile showing the location of field sites, including the control site at Salar Grande where all halite nodules originated (**A**), and the transplant sites at ALMA (**B**), Yungay (**C**), and Chañaral (**D**). *Right* Photos of each site showing the halite nodules and the environmental sensors deployed 1 m off the ground (black arrows). Additional photos of halite nodules and the sensors installed inside are in Fig. S1.

whereas they are mostly absent in other endolithic or hypolithic communities, and BSCs[2,3]. Finally, the halite communities are dynamic and capable of responding rapidly to sudden and severe changes in environmental conditions[10]. This characteristic may explain differences in community composition within an evaporitic deposit over spatial scales of hundreds of meters to tens of kilometers[14] and between evaporitic deposits throughout the hyper-arid core[4,15].

Halite communities are confined to a relatively small volume within a nodule (typically 20 to 50 cm in size) and, as such, each nodule represents a self-sustained microcosm that relies on limited, if any, exchange of biomass with the surrounding environment. This confinement offers a unique opportunity to relocate whole communities to different climate regions in the desert (e.g., colder, drier, higher solar irradiance) by transplanting entire halite nodules without disturbing the community within. Consequently, the entire community's response to the new environment can be monitored at the community level using molecular techniques. Few microbial ecosystems can be forced into new climate conditions and monitored at a different location over long periods. This paper presents the result of such a transplant experiment.

Results

Halite nodules from Salar Grande (control site) were transplanted to three other sites in the Atacama Desert, namely ALMA, Yungay, and Chañaral (Fig. 1, Fig. S1). We analyzed the environmental data collected at each site and the microbial communities' taxonomic and functional changes a year later.

Environmental data analysis. Different sites showed contrasting air humidity conditions RH_{air} (Fig. S2). In Salar Grande (638 masl), the maximum daily RH_{air} was above the 95% threshold for 85 days over the collection period, and the minimum daily RH_{air} values oscillated around 25%. In contrast, the ALMA site (2885

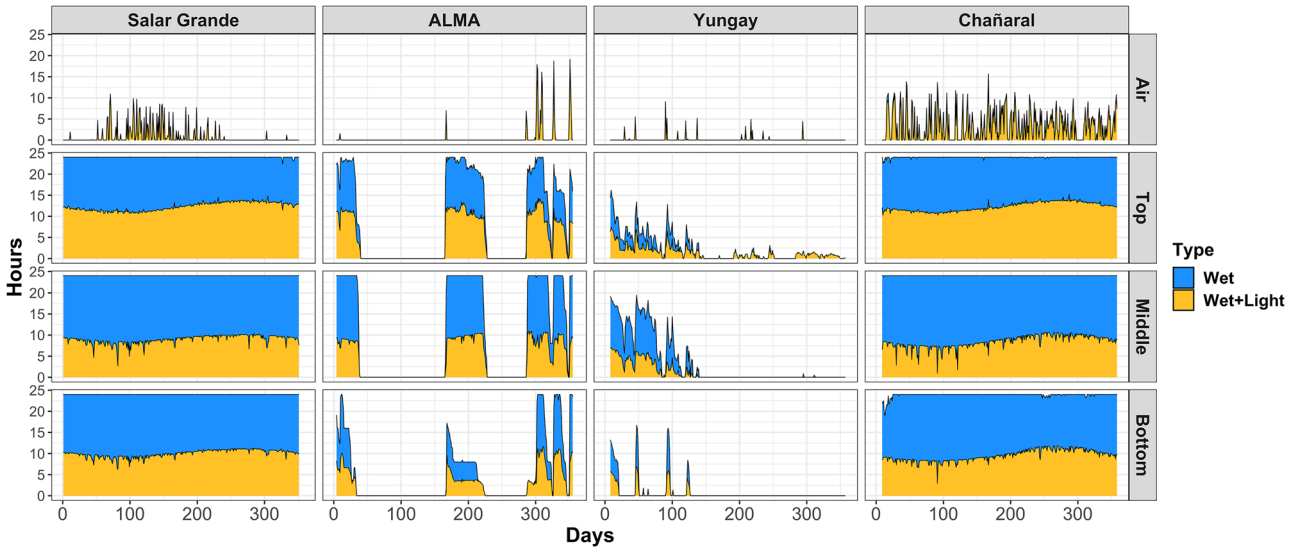

Figure 2. Daily hours of wet and wet + light conditions throughout data collection in the air and inside the halite nodules at each site. Salt deliquescence enables wet conditions inside halite nodules at RH > 75%. In the air, wet conditions occur at RH > 95%. Wet + light conditions occurred when RH values above respective thresholds co-occur with PAR > 0.01µmol photons m^{-2} s^{-1}.

masl) exhibited a dry regime with maximum daily RH_{air} above 95% for only 24 days and minimum daily RH_{air} values around 10%. The ALMA site also experienced three events of atmospheric precipitation (rain or snow) at approximately days 10, 160, and 280 after the transplant. During the wetting events at days 10 and 280, minimum daily temperatures were above 10 °C, whereas they fell below 0 °C during the wetting event at day 160. The Yungay site (953 masl) recorded the most variable T_{air} and RH_{air} readings. RH_{air} values were generally low throughout data collection with mean values above 50% on only 15% of collected days and only 16 days recorded with RH_{air} values ≥ 95%. The Chañaral site (848 masl) was similar to Salar Grande but with more variable daily values for RH_{air} and slightly cooler daily temperatures. Chañaral recorded 239 days with peak RH_{air} ≥ 95%.

Humidity conditions inside halite nodules (RH_{halite}) varied significantly between sites (Fig. S3B). At Salar Grande, the mean RH_{halite} remained near 75% for the entire recorded period. No differences were observed between the top, middle, and bottom sections of the nodules. At the ALMA site, the mean RH_{halite} was initially high (75%) but dropped to values around 25% approximately 50 days after the transplant. At around day 160, corresponding to a wetting event recorded by the atmospheric sensor (RH_{air}), the mean RH_{halite} suddenly increased to 75%. The RH_{halite} remained at 75% for 65 days and subsequently dropped over a period of 55 days to reach values around 25%. At approximately day 280, corresponding to another atmospheric wetting event, a second spike in the mean RH_{halite} to 75% was observed. Values remained high, albeit variable, until the end of the recorded period. Minor differences were observed between the top, middle, and bottom sections of the nodules. At the Yungay site, the mean RH_{halite} was initially high (c.a. 75%) but quickly declined to values between 50 and 60%. The mean RH_{halite} oscillated between those values for most of the recorded period, except for short intervals when it dropped to values close to 25%. Similar to ALMA, minor differences were observed between the nodules' top, middle, and bottom sections. In the Chañaral site, the mean RH_{halite} values remained constant near 75% for the entire recorded period, which was similar to the control site in Salar Grande. Temperature conditions inside the nodules were similar at all sites and comparable to the air temperature (Fig. S3A). These findings indicated that the mean RH_{halite} values point to the continuous presence of saturated NaCl brines filling the pore spaces of the halite nodules in Salar Grande and Chañaral. In ALMA, halite nodules went through three "wet periods" when mean RH_{halite} values were consistent with the presence of saturated NaCl brines (RH_{halite} = 75%), interspaced with two "dry periods" when mean RH_{halite} remained low. In Yungay, halite nodules progressively dried out with no observable wet/dry cycling.

Daily cumulative hours of wet and wet + light conditions further emphasized the different environmental regimes experienced by communities inside transplanted nodules compared to nodules at the control site (Fig. 2). At Salar Grande and Chañaral, conditions inside the nodules (top, middle, and bottom) were compatible with metabolic activity, both heterotrophic (wet) and photosynthetic (wet + light) for the entirety of the recorded period. In contrast, at the ALMA site, conditions inside the nodules (top, middle, and bottom) were only compatible with metabolic activity within three separate periods, each lasting 50–65 days and separated by dry spells lasting 50–100 days. At the Yungay site, conditions inside the nodules (top and middle) were compatible with metabolic activity at the beginning of the transplant experiment but slowly declined during the first 150 days. After that, only the top of the halite nodules experienced brief periods compatible with metabolic activity lasting several hours.

Long periods of extreme dryness favored *Halobacteria*. We investigated changes in the microbial community structure and function inside the transplanted halite nodules using high-throughput molecular

methods (Fig. S4). After 1 year, there was an increase in the ratio of archaea to bacteria in the ALMA transplant community and, to a lesser extent, in the Yungay transplant community, based on both contig and MAG assemblies (Fig. 3A,B, respectively). In contrast, this ratio in the transplant community at Chañaral remained the same as that of the native community at Salar Grande. The higher archaeal relative abundance at ALMA resulted from an increase in the relative abundance of *Euryarchaeota* (represented mainly by *Halobacteria*) to ~ 80% of all contigs compared to ~ 60% in the Salar Grande native community (Fig. 3C, Dataset S1). In contrast, Cyanobacteria decreased significantly at ALMA compared to Salar Grande from ~ 6 to ~ 3% (Welch's t-test $p < 0.05$, for Contigs and MAGs). *Bacteroidetes* (mostly *Salinibacter*) relative abundances were also lower at the ALMA and Yungay sites than those observed at Salar Grande and Chañaral, although not statistically significant. The same patterns were recapitulated using MAG relative abundances (Fig. 3D, Dataset S1). Overall, the variance in the data was higher in Yungay, potentially as the result of sample outliers (Fig. 3E,F). Ordination plots of Bray–Curtis distances showed the clustering of ALMA and Yungay transplant communities in one group and Salar Grande native and Chañaral transplant communities in another group when using contig and MAG assemblies (Fig. 3E,F). Although some samples such as SG2 (for contigs) and CH1 (for MAGs) appeared to be outliers, the groupings described above were statistically significant (ANOSIM $p < 0.05$ for both).

Extreme dryness impacted the functional potential of halite communities. The functional potential of the halite communities was determined for each location using functional annotation from the KEGG Brite pathways (Fig. 4A). Overall, proteins for transport pathways such as peptide/nickel, branched amino-acids, and ABC-2 type transport systems were the most abundant in communities across all sites. Notably, the relative abundances for peptide/nickel transport systems and a HTH-type bacteriorhodopsin transcriptional activator were higher in the ALMA community when compared to other transplanted or native communities. Bacteriorhodopsin is particularly relevant to haloarchaea because it is a light-activated proton pump that can supplement the ATP budget of the cell[16]. We also found a significant decrease in the isoelectric point of the translated proteome of the ALMA community (Welch's t-test, $p < 0.05$) together with an increase in potassium transport potential (*tr*K genes relative abundance) (Fig. 4B,C). These adaptations are hallmarks of salt-in-strategists, which accumulate intracellular KCl to balance the high osmotic pressure of their environment, and were consistent with the observed increase in relative abundance of haloarchaea at the ALMA site.

Few specialized MAGs dominated halite communities. One hundred and four good quality MAGs (completeness ≥ 70% and contamination ≤ 5%) were recovered from the halite community metagenomes after binning, quality filtering, and dereplication (Dataset S2). Taxonomy annotation at the phylum level revealed that most MAGs belonged to the *Euryarchaeota* (69/104 MAGs). The changes in relative abundance of most of the MAGs were site-specific (Fig. S5). We also found six MAGs that were highly abundant in at least one site and showed the highest changes in relative abundance between the control site (SG) and the transplanted sites. We called them "specialized MAGs"; MAG.i.4, MAG.i.34, and MAG.i.36 were annotated as *Euryarchaeota*, MAG.i.2, and MAG.i.39 were annotated as *Bacteroidetes*, and MAG.i.27 was annotated as *Cyanobacteria* (Fig. 5A).

Deeper taxonomic identification of the specialized MAGs with the GTDB-tk (ANI > 98% with the closest relative MAG in the GTDB; Table S1) showed that the archaeal MAGs were exclusively represented by *Halobacteriales* and included *Natronoarchaeum* (MAG.i.4), *Halococcus* (MAG.i.34), and *Halorussus* (MAG.i.36) genera (Fig. S6A). The *Bacteroidetes* MAGs belonged to the *Salinibacteraceae* family and were clustered with unidentified genomes related to *Salinibacter* (MAG.i.2) and *Salisaeta*/*Logimonas* (MAG.i.39) genera (Fig. S6B). The cyanobacterial MAG (MAG.i.27) belonged to the *Rubidibacter* genus and was closely related to the *Halothece* and *Euhalothece* genera (Fig. S6C). The increased relative abundance of the specialized MAGs was site-specific. For example, *Halococcus* and *Natronoarchaeum* MAGs relative abundance was ~ 18% and ~ 11% at ALMA, respectively, compared to ~ 9% and ~ 0.9%, respectively, in the native nodules of Salar Grande and the transplants of Yungay and Chañaral (Fig. 5A). The relative abundance of *Halorussus* MAGs also increased from ~ 0.7% in Salar Grande native nodules to ~ 4% in ALMA and ~ 7% in Yungay transplants. There were also MAGs that decreased in relative abundance after the transplant. *Salinibacter* MAGs decreased from ~ 13% in Salar Grande native nodules to ~ 8% in the ALMA and Yungay transplants, and *Rubidibacter* MAGs declined from ~ 10% in Salar Grande native nodules to ~ 3% in ALMA transplants (Fig. 5A).

Protein encoding genes for osmoregulation were identified in the specialized MAGs with distribution indicating different osmoadaptation strategies. All the archaeal MAGs (MAG.i.4, MAG.i.34, and MAG.i.36) encoded ion transport proteins, including for a sodium: solute symporter of the SSS family and for the Trk potassium transport system (*trk*H and *trk*A), both of which are functional traits of salt-in strategists. These MAGs also encoded genes for a glycerol kinase (*glp*K) that catabolizes glycerol to glycerol-3-phosphate (G3P) and a G3P dehydrogenase (GlpA, GlpB, GlpC), potentially conferring the ability to use glycerol as a carbon source[17]. *Halococcus* (MAG.i.34), the most abundant MAG in ALMA transplants, also encoded genes for the uptake of several compatible solutes; these included genes for a OpuC transporter for a broad spectrum of compatibles solutes including choline, ectoine, glycine-betaine, OpuA and OpuD transporters for glycine-betaine, OpuBD for choline, and BetT for choline, glycine-betaine, and proline[18] (Fig. 5B). In contrast, these genes were not found in *Natronoarchaeum* (MAG.i.4) and *Halorussus* (MAG.i.36). MAGs from the *Salinibacteraceae* (MAG.i.2 and MAG.i.39), also salt-in strategists, encoded genes for a sodium: solute symporter and the Trk potassium transport system. The *Rubidibacter* MAG (MAG.i.27) encoded for genes for trehalose biosynthesis such as *glgA* (starch synthase), *glgC* (glucose-1-phosphate adenylyltransferase), and *treX* (isoamylase)[19]; and ectoine biosynthesis such as *asd* (aspartate-semialdehyde dehydrogenase), *ectB* (diaminobutyrate-2-oxoglutarate transaminase), and *lysC* (aspartate kinase)[20].

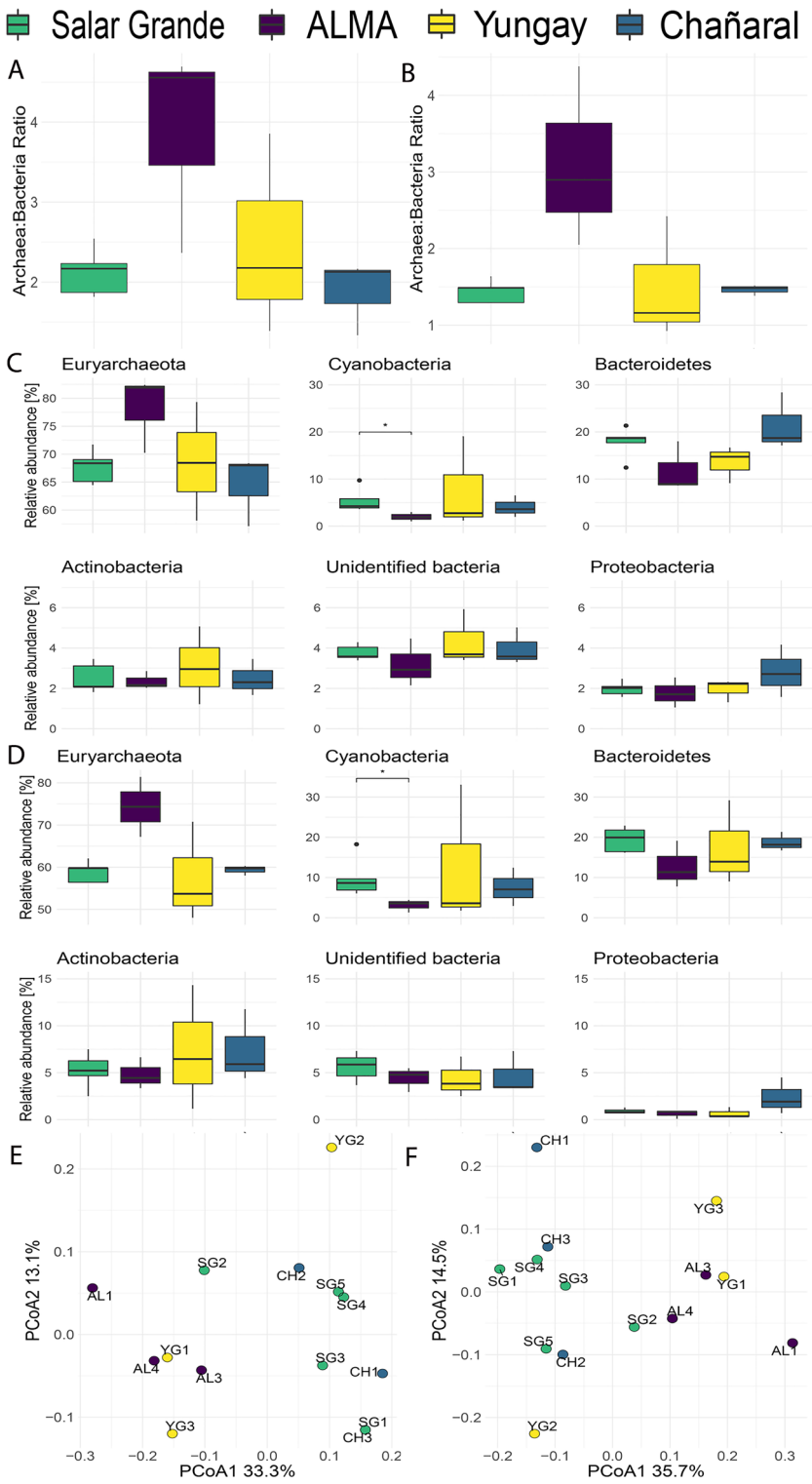

Figure 3. Relative abundances of halite microbial taxa across sites showing changes in community taxonomic composition after 1-year exposure to different environmental conditions. Archaea: bacteria ratios in (**A**) contigs and (**B**) MAGs. Relative abundances at the phylum level in (**C**) all contigs and (**D**) MAGs. Bray–Curtis distance's ordination plots calculated on the relative abundances of (**E**) contigs and (**F**) MAGs across sites. Error bars represent standard deviation; significance bars denote Welch's t-test $p < 0.05$.

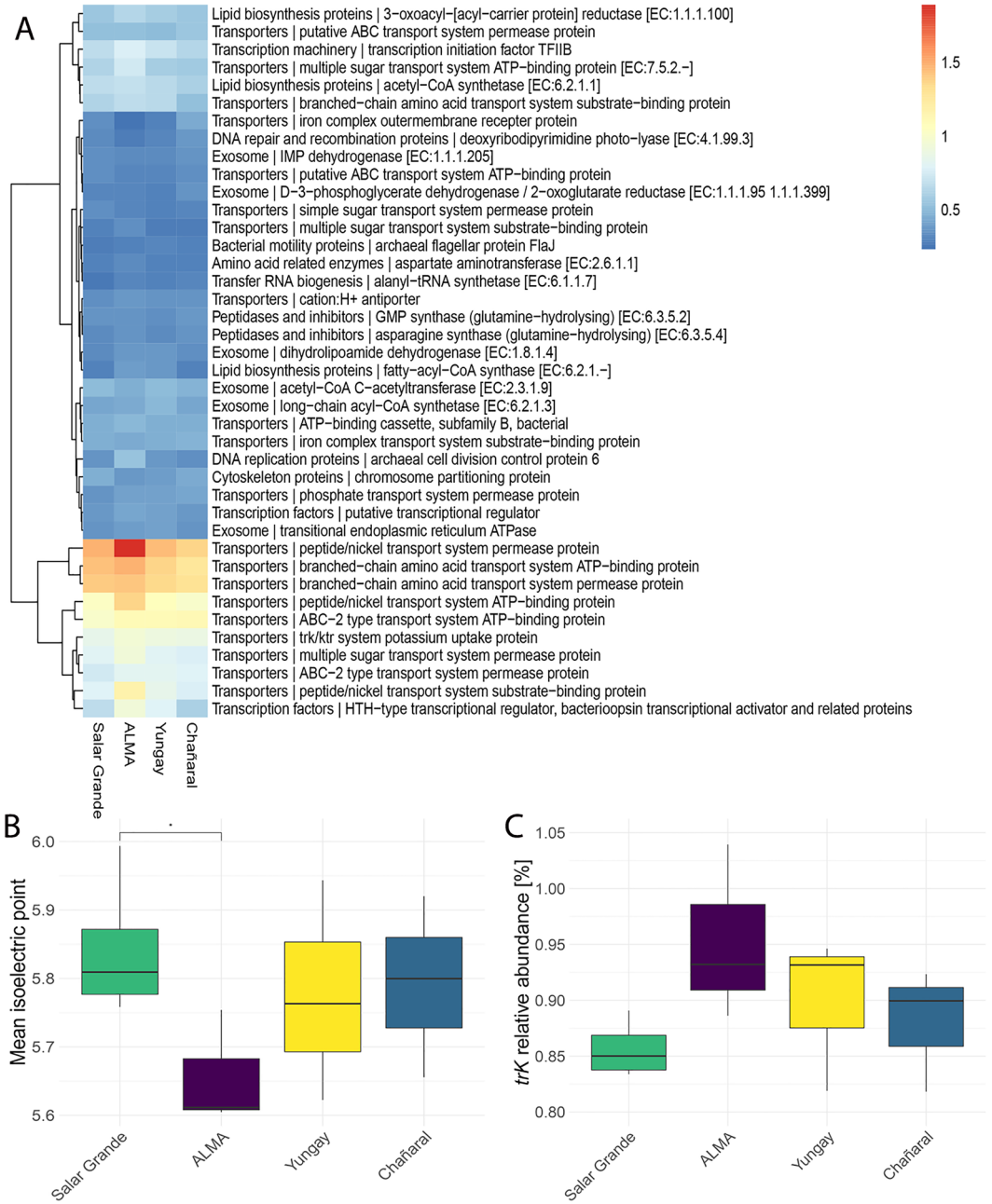

Figure 4. Functional changes across sites 1 year after transplantation of halite nodules represented by (**A**) relative abundances of the 40 most abundant KEGG Brite pathways in all contigs; color-coded legend is in %. (**B**) Weighted average of predicted protein isoelectric points of proteins encoded in all contigs. (**C**) Potential potassium uptake inferred from *trK* genes relative abundance quantified in all contigs.

***Dolichomastix* and *Halovirus* relative abundances across sites.** Algal contigs, assembled from the halite metagenomes, belong to a unique alga, *Dolichomastix,* whose MAG was previously reported from Salar Grande[21]. We quantified *Dolichomastix* relative abundance at each site by mapping sequence reads to the genome sequence assembled in 2021. There was no statistical difference in the relative abundance of *Dolichomastix* across sites; however, its mean relative abundance was lower in the ALMA and Yungay communities (~ 13%) than those of Salar Grande and Chañaral (14.5%) (Fig. 6A).

Using virsorter2, we found 571 viral contigs across all samples. Of these, 101 were annotated as *Halovirus* with Cenote-Taker2, 119 were unknown viruses, and 334 were unknown phages. The relative abundance of all viral contigs was similar across all sites (Fig. S7, Dataset S3); however, the relative abundance of *Halovirus,* the most abundant known virus family in the halite communities, varied across sites. There was an increase in *Halovirus* relative abundance in ALMA and Yungay that correlated with the increase in the relative abundance of haloarchaea at those sites (Fig. 6B).

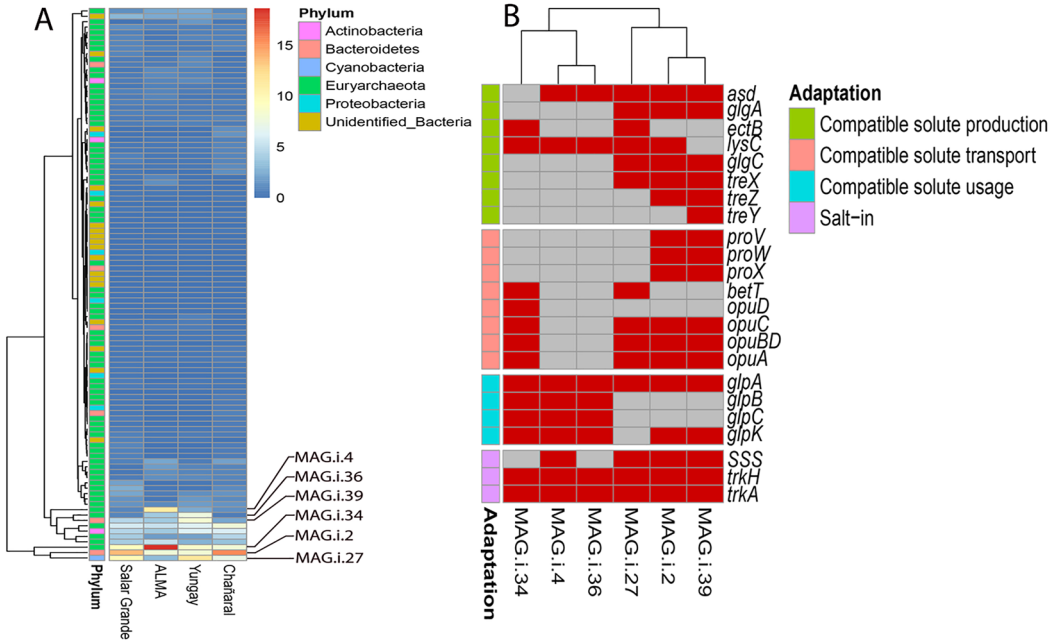

Figure 5. Taxonomic and functional characterization of MAGs across sites. (**A**) Taxonomic annotation and relative abundance of MAGs across sites; labeled are the most abundant site-specific MAGs; color-coded legend is in %. (**B**) Presence (red boxes) and absence (grey boxes) of genes involved in compatible solute production, transport, and utilization in the site-specific MAGs.

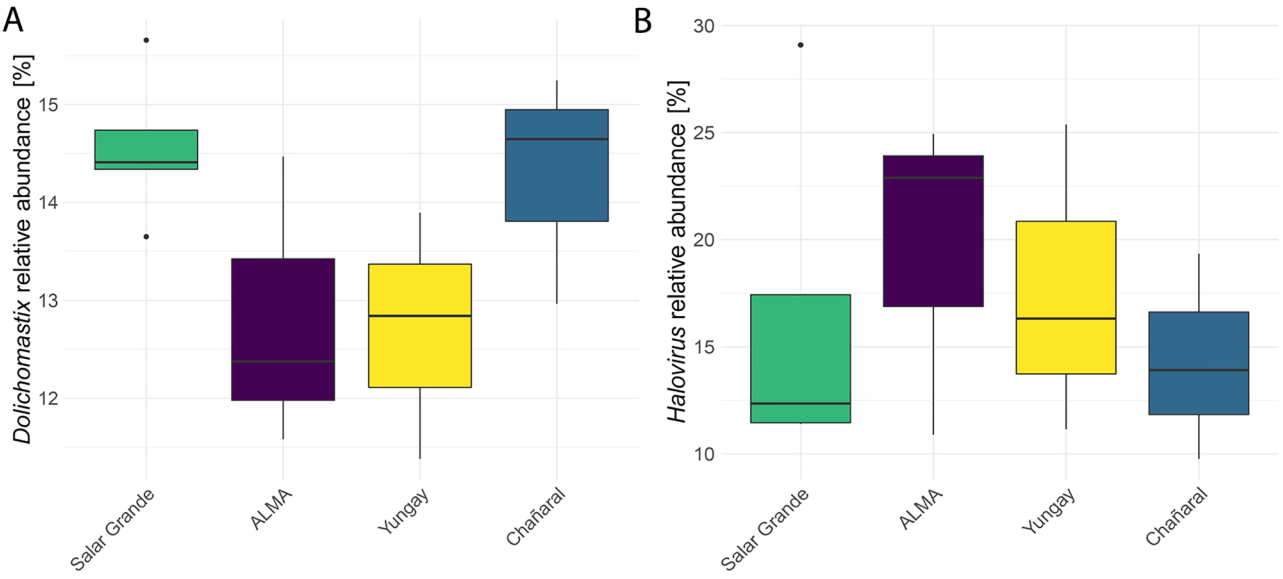

Figure 6. Algal and viral contigs quantification. (**A**) Relative abundance of *Dolichomastix* genomes in the halite communities, and (**B**) *Halovirus* contigs relative abundance across sites. Standard deviation is represented by error bars and the significance tested by Welch's t-test.

Discussion

Transplanting halite nodules to different sites of the Atacama Desert triggered an adaptive response of the halite community, leading to changes in taxonomy, cellular and biochemical properties related to local environmental conditions. All the halite nodules transplanted from Salar Grande contained liquid brines in their pore spaces, as evidenced by the high RH_{halite} values at the start of the experiment. After the transplants, dry conditions and specific wetting events resulted in three distinct periods of water availability inside the nodules at ALMA. In contrast, halites at Yungay showed a progressive loss of water available to microorganisms, followed by a

protracted period of desiccation. Halite nodules at Salar Grande and Chañaral maintained their water content for the entire duration of the experiment.

Water dynamics inside the nodules had an apparent effect on the composition and functional adaptations of the halite communities, with archaea and bacteria showing different trends. *Euryarchaeota*, mainly *Halobacteria,* the dominant taxon at Salar Grande, increased significantly in abundance at the sites where moisture content decreased over time (ALMA and Yungay), while it remained unchanged at Chañaral, where moisture content stayed the same. However, reduced water availability did not affect all *Halobacteria* in the same way; *Halococcus*, *Halorussus*, and *Natronoarchaeum* were the main taxa that increased in relative abundance at the driest sites. On the other hand, *Bacteroidetes,* mainly represented by *Salinibacter,* was the dominant bacterial group at Salar Grande and showed a slight decline at the drier sites (ALMA and Yungay). A reduction in *Bacteroidetes* abundance was also noted by Robinson et al.[4] when comparing halite communities from Salar Grande with native halite communities at the drier Yungay site. However, Uritskiy et al.[10] reported an increase in the relative abundance of *Bacteroidetes* in halite nodules at Salar Grande with increasing water availability after a rainfall. The observed trends recapitulate the changes in community structure observed elsewhere along salinity gradients, with haloarchaea dominating at the highest salinities (lower water content), while the relative abundance of *Bacteroidetes* remains mainly unchanged[22,23]. It is important to note that halite nodules are largely self-sustained and closed systems with limited input or dispersion[14]. Therefore, the halite community observed after a 1-year transplant was a subset of the original community in Salar Grande, with little to no import from the environment.

Cyanobacteria were also affected by changes in water availability, with a decline in relative abundance at the ALMA site but an increase at the Yungay site. The latter is consistent with Robinson et al.[4] showing that *Cyanobacteria* were more abundant in native halite nodules at the Yungay site than at the Salar Grande site and supports the notion that these photosynthetic microorganisms are generally well adapted to extreme dryness[14]. Their decline at the ALMA site appears counter to that argument but may be explained by the higher energy demand imposed by wet/dry cycling (see below) compounded by the colder conditions at this site. We also found a decrease in the *Dolichomastix* algae's relative abundance at the driest sites indicating a potential dry limit for eukaryotes, as previously reported[4]. Metagenomes from all sites harbored viral contigs but most had only remote similarity to viral genomes found in public databases. Remarkably, Polinton-like viruses were detected albeit at very low abundances. These are large mobile genetic elements found in diverse eukaryotic genomes, including algal genomes, and in environmental metagenomes[24]. This finding suggests that the only eukaryote in the system, the *Dolichomastix* algae, may be the host of these viruses.

Wet/dry cycling is a significant stressor for all organisms, even for desert organisms specialized to survive extreme dryness[25,26]. Inside halite nodules, wet/dry cycling also causes important salinity and osmotic pressure changes. Changes in salt concentration are energetically expensive. Consequently, the amount of energy generated during dissimilatory metabolism and the mode of osmotic adaptation are strong selective factors in environments with high (and fluctuating) salt content[27]. The observed increase in the relative abundance of salt-in strategists, although primarily members of the archaea, in transplants at the ALMA site, and, to a lesser extent, at the Yungay site are consistent with the need to maximize cellular bioenergetics when confronted with changes in water availability. Indeed, the salt-in strategy has a lower energy cost than other adaptations to high osmotic pressure, such as salts extrusion and compatible solutes, which requires the active synthesis or uptake of compounds such as sugars, polyols, and amino acids[27]. The advantage of salting-in should be more decisive in environments where organisms go through multiple wet/dry cycles over a relatively short time, like at the ALMA site, since such fluctuations are energetically taxing. But the use of compatible solutes might also be effective in situations where organisms progressively dry out and then remain desiccated, as was observed at the Yungay site because organisms have ample time and energy to synthesize compatible solutes. This latter point would explain the observed decline of *Cyanobacteria* at the ALMA site (wet/dry cycling; higher energy cost) and their relative increase at the Yungay site (progressive desiccation; lower energy cost). Despite being salt-in strategists, *Bacteriodetes* decreased in abundance at the driest sites; indeed it was previously reported that at the highest salt concentrations, an increase in *Euryarchaeota* relative abundance was correlated with a decline in *Bacteroidetes* relative abundance[28–30]. The vast increase in abundance of haloarchaea at the driest sites most likely outcompeted the adaptation potential of a few genera or families of *Bacteriodetes* salt-in strategists.

The increasing dominance of salt-in strategists at the ALMA site was also reflected in the functional potential of the halite communities. Salt-in strategists take up KCl to balance the high osmotic pressure of their environment[16,31], and *trK* transport systems are essential in obtaining the high cytoplasmic concentration of K found in these microorganisms[26,32]. Consequently, we saw an increase in the relative abundance of *trK* genes in the ALMA and Yungay communities, with a more significant increase at ALMA consistent with the succession of wet/dry cycles compared to the gradual decline in water content observed at Yungay. A function related to energy production that was found enriched in the ALMA community transplants was the *HTH* transcriptional activator of bacteriorhodopsin. Bacteriorhodopsin is an essential protein complex in haloarchaea that acts as a light-dependent proton pump to supplement the energy budget of haloarchaea; it illustrates another adaptive strategy to meet the energetic demands at high and fluctuating salt concentrations[16]. The adaptive advantage of salt-in strategists was also reflected in the lower isoelectric point values measured in the predicted metaproteome of ALMA transplants (mean pI ~ 5.4 in comparison of ~ 5.8 at other locations). The proteins of salt-in strategists proteins are enriched in acidic amino acid residues at their surface compared to their non-halophilic homologs to maintain stability and activity at high salt concentrations[10,33,34]. The same dynamic was reported in other extreme environments where the dominance of salt-in strategists, *Euryarchaeota* and *Salinibacter*, was correlated with lower isoelectric point values of the community's metaproteome[10,30,35].

Poor nutrient availability is another constraint for communities that rely on the primary production of *Cyanobacteria* and algae, as is the case in halite nodules[5,6,14]. Haloarchaea mainly use amino acids as carbon sources[36], transported inside the cell by ABC-type transporter systems. ABC-type transporters were the most abundant

pathways across all halite communities, and those related to peptide/nickel transport increased in response to water loss in the ALMA and Yungay transplants. MAGs functional analysis also revealed enrichment of pathways for using glycerol and other compatible solutes as carbon sources at the driest sites[37,38].

These findings support the conclusion that opportunistic salt-in strategists took over the halite communities at the driest sites. They most likely benefited from carbon sources, such as glycerol, choline, ectoine, glycine-betaine, and proline, newly released in the environments by the death of microorganisms the least adapted to desiccation or wet/dry cycling and colder conditions recorded at Yungay and ALMA, respectively. These opportunist salt-in strategists were all members of the archaea and were site-specific, harboring the functional potentials best adapted to the new environmental conditions following the transplant. The decrease in relative abundance of cyanobacteria, algae, and *Bacteriodetes* we observed at the driest sites supports this idea. Drastic changes in halite communities were previously reported, albeit in the opposite direction, resulting from a massive rain event[10]. Furthermore, archaeal uptake of glycerol from dead *Dunaliella* cells was documented in halite cores from the Death Valley, California[39] and the Saline Valley, California[40]. The *Dolichomastix* algae from Salar Grande could potentially accumulate large amounts of glycerol to balance the high osmotic pressure of its environment[16], this glycerol could then be released when environmental conditions deteriorate and cell death occurs, benefiting opportunistic microorganisms.

In conclusion, 1-year transplants showed that decreasing water availability was energetically more costly to the halite communities, particularly at the ALMA site, where communities experienced several cycles of hydration and dehydration. These extreme conditions favored opportunistic salt-in strategists equipped with mechanisms for energy conservation under high salt, such as the intracellular accumulation of KCl, the use of light-dependent proton pumps, and the ability to consume metabolites released from dead community members. Our work underscores how those fluctuations in water availability are important drivers of community structure and functional adaptations in the halite niche.

Methods

Experimental design and sampling. Salar Grande (20.95 S, 70.02 W; 638 masl) was chosen as the "control site" for the transplant experiment. Halite microbial communities have been extensively characterized at this site and represented a suitable baseline[4,5,10,14,21]. In February 2018, halite nodules were transplanted from Salar Grande to the ALMA observatory on the Altiplano (23.07 S, 67.98 W; 2885 masl), the hyper-arid Yungay region (24.05 S, 69.9 W; 953 masl), and the less arid Chañaral region in the southern part of the desert (26.17 S, 70.3 W; 848 masl) (Fig. 1). For each transplant, 8 nodules (3 nodules with environmental sensors and 5 nodules for metagenomic analyses) were collected within an area < 100 m^2. Eight nodules were marked in Salar Grande as controls. In March 2019, five transplanted nodules were harvested in the field at each site, and weather data were collected from all data loggers (see below). The nodules were cut in half with a circular saw, and the colonization zone was scrapped with a sterilized knife. The resulting grounded halite was collected in sterile Whirl–Pak bags and placed in dark and dry conditions for transportation and storage until analysis.

Environmental data analysis. Atmospheric relative humidity (RH_{air}) and temperature (T_{air}) were recorded with HOBO Pro v2 External T/RH Data Loggers installed 1 m above the ground at each of the four sites. Photosynthetic light was recorded at ground level at each site with a HOBO PAR (photosynthetic active radiation) sensor that measures light intensity in the range 0–2500 µmol m^{-2} s^{-1} over wavelengths from 400 to 700 nm. Halite temperature (T_{halite}) and relative humidity (RH_{halite}) were measured inside three transplanted nodules at each site using the same HOBO Pro v2 External T/RH Data Loggers. Sensors were installed at the top, middle, and bottom of the nodules by drilling three separate holes and sealing the sensor with resin as previously described[14] (Fig. S1). All sensors were set to collect data every 30 min.

Data points for T, RH, and PAR were aligned to the same times on each recorded day by modeling raw data time-series and estimating values at 3-min intervals, starting at midnight. Generalized additive models (GAMs) were built for T, RH, and PAR with adaptive smooths of the time of day expressed as day-hours in 3 min intervals and maximum likelihood based optimization of the smoothness parameters[41]. Models were implemented with the GAM package[42] in R (version 4.1.0). Daily total values for environmental variables were calculated independently for each sensor. Mean values between replicate halite nodules were reported for top, middle, and bottom positions.

The daily dynamics of T, RH, and PAR were used to calculate cumulative daily hours of wet and wet + light periods inside and outside halite nodules as proxies for potential metabolic activity. We assumed water was available to the halite communities when $RH_{halite} \geq 75\%$, the equilibrium relative humidity of a saturated NaCl brine[8]. For PAR, we used PAR ≥ 0.01 µmol photons m^{-2} s^{-1} as the absolute minimum irradiance required by highly adapted primary producers[43]. We calculated the cumulative daily hours of wet and wet + light periods outside the nodules by assuming a RH_{air} threshold ≥ 95% and PAR ≥ 0.01 µmol photons m^{-2} s^{-1}. The RH_{air} threshold value is based on the observation that fog water collection in the Atacama Desert can occur at RH_{air} values slightly lower than 100%[44] and to account for possible dew deposition[45]. For each day, the cumulative number of wet and wet + light hours were generated as a sum of 3-min intervals at which values for RH and PAR exceeded respective thresholds.

DNA extraction and sequencing. Total DNA was extracted from 2 to 5 g of grounded halite using the DNeasy Powersoil DNA extraction kit (QIAGEN). The DNA was cleaned with 3× AMPure XP Beads (Beckman Coulter) before library construction. The KAPA HyperPlus kit (Roche) was used to construct the genomic libraries with 10 ng of DNA, following the manufacturer's instructions and with the DNA from each nodule barcoded separately. Final library size selection was made with 0.5× and 0.7× KAPA HyperPure beads (Roche)

ratio to recover fragments 300–500 bp in length. Five libraries for Salar Grande and 3 for the other locations were paired-end sequenced by Novogene (https://en.novogene.com/) with 150 bp reads length using the Illumina NovaSeq 6000 platform.

Sequences quality filtering, assembly, and binning. Sequence quality control, assembly, annotation, and quantification of contigs were performed using the MetaWRAP pipeline v1.3.2[46]. Raw reads were trimmed, and human contamination (1,309,206 reads corresponding to 0.47% of all reads) was removed using the read_qc module with default parameters. Two strategies for metagenome-assembled genomes (MAGs) assembly and binning were implemented (Fig. S4). The first strategy retrieved the less abundant MAGs as recommended in the metaWRAP workflow; reads were concatenated in a single file, assembled into contigs with the metaWRAP's assembly module using MEGAHIT[47], and binned into MAGs with the binning module using METABAT2[48]. The second strategy retrieved the most abundant MAGs; data from each sample were assembled individually to contigs using METASPADES[49] and binned into MAGs using METABAT2. MAGs obtained from the two assembly strategies were pooled and de-replicated using dRep v2.0.0[50] to get the most representative MAG for each species. Genomes were filtered by quality according to completeness (≥ 70%) and contamination (≤ 5%) using CheckM[51]. MAGs with an average nucleotide identity ≥ 95% and a coverage threshold ≥ 10% were considered the same species[52].

Taxonomic annotation and diversity analysis. Contigs and MAGs were quantified and normalized to sample size using the quant_bins module from metaWRAP. The resulting tables were transformed to relative abundance expressed as the percentage of each contig or bin in its sample using the vegan package in R[53]. Specifically, relative abundance was calculated by dividing the normalized counts for each contig/MAG by the sum of the counts for all contigs/MAGs per nodule and per location; Taxonomic annotation at the phylum level was performed with contigs and MAGs using the classify_bins module in metaWRAP and the NCBI nucleotide database v4.0. Phyla relative abundances were calculated for each site, ratios of archaea to bacteria were calculated by dividing relative abundances for each site, and the results were visualized by boxplots. Significance of differences for means of archaea: bacteria ratio and phyla relative abundances were evaluated using Welch's t-test. The Bray–Curtis index for each site was calculated using the vegan package. Distance matrices were visualized in PCoA plots generated with the ape R package[54]. The significance of clusters in PCoA plots was assessed with the ANOSIM statistic calculated in vegan.

Functional annotation. Contigs obtained from the METASPADES assemblies were uploaded to the Integrated Microbial Genomes/Metagenomes from the Joint Genome Institute (JGI IMG) v5.0.0 service[55]. Gene copy counts were downloaded from the server with their assigned KO terms list and linked to their respective KEGG BRITE pathway classification. Counts were normalized by dividing by the number of reads in the corresponding sample and transformed to relative abundance using vegan. The 40 most abundant pathway relative abundances were visualized in a heatmap using the pheatmap R package. The average isoelectric point (pI) was calculated for each metagenomic assembly; open reading frames (ORFs) were predicted with PRODIGAL[56] using the annotate_bins module from metaWRAP, and the pI for each ORF was calculated using ProPAS[57]. For potassium transport potential (*tr*K genes), relative abundance of contigs annotated with the KOs: K03498 and K03499 were retrieved from the annotation table for each sample and visualized by boxplots. Significant differences among locations were assessed with Welch's t-test for the pI and trK relative abundances.

Specialized MAGs characterization. Specialized MAGs were defined as those with a mean relative abundance higher than 10% in at least one site; they were selected to be classified at a deeper taxonomic level (Dataset S3). Selected genomes were uploaded to GTDB-tk server[58] to be taxonomically classified with the Genome Database Taxonomy (GTDB)[59]. Closely related MAGs at the family level were retrieved from the GTDB for phylogenomic tree construction using GTOTree v1.6.11[60] with MUSCLE alignment of single-copy genes (SCP) in the HMM database and FastTree algorithm for tree construction.

Potential osmoadaptation strategies for specialized MAGs were obtained by uploading protein prediction from annotate_bins in metaWRAP to the GhostKOALA server and retrieving the list of KO identifiers for each MAG[61]. KO lists were linked to (1) osmoadaptation KO genes lists based on gene lists from Wong et al.[62] and (2) the utilization of glycerol as a carbon source based on gene lists from Wong et al.[62] and Oren[38], respectively. Occurrences of osmoadaptation strategies and use of glycerol were represented in a heatmap indicating the presence or absence of each gene in the selected MAGs.

Algal and viral contigs quantification. The *Dolichomastix* alga genome, previously assembled by Uritskiy et al.[21], was retrieved from github (https://github.com/ursky/metatranscriptome_paper/tree/master/MAGS). Its representation in each sample, as genome copies per million of reads, was calculated using the quant_bins module from MetaWRAP and transformed to relative abundance using vegan in R; significance of variation across sites was calculated using Welch's t-test.

Halite communities assembled contigs obtained from METASPADES assemblies were used for viral identification of dsDNA viruses, *Nucleocytoviricota* (NCLDV), and *Lavidaviridae* viruses using virsorter2[63]. Contigs were quality checked with CheckV[64] and contigs > 95% identity and > 85% coverage were taxonomically annotated with Cenote-Taker2 using default parameters[65]. Viral contig relative abundances were calculated by linking the contig annotation from Cenote-Taker2 with the contig depth obtained with metaWRAP quant_bins module. Variation of virus relative abundance across locations was represented in boxplots, and the significance was assessed using Welch's t-test.

Data availability

Raw sequences are available at the National Center for Biotechnology Information (NCBI) under the BioProject ID PRJNA808683. BioSample accession numbers are: SAMN26101366–SAMN26101368 for ALMA, SAMN26101369–SAMN26101371 for Chañaral, SAMN26101372–SAMN26101376 for Salar Grande, and SAMN26101377–SAMN26101379 for Yungay. All analysis pipelines, processed data, analysis and visualization scripts, and reconstructed MAGs are available at https://github.com/capfz200/Halite_paper. The metagenome assembly and functional annotation are available in the Joint Genome Institute (JGI) Integrated Microbial Genomes and Microbiomes portal under the GOLD Study ID https://gold.jgi.doe.gov/study?id=Gs0154137.

Received: 26 March 2022; Accepted: 31 October 2022
Published online: 21 November 2022

References

1. Pointing, S. B. & Belnap, J. Microbial colonization and controls in dryland systems. *Nat. Rev. Microbiol.* **10**, 551–562 (2012).
2. Wierzchos, J., Ríos, A. D. L. & Ascaso, C. Microorganisms in desert rocks: The edge of life on Earth. *Int. Microbiol.* **15**, 171–181 (2012).
3. DiRuggiero, J. *et al.* Microbial colonisation of chasmoendolithic habitats in the hyper-arid zone of the Atacama Desert. *Biogeosciences* **10**, 2439–2450 (2013).
4. Robinson, C. K. *et al.* Microbial diversity and the presence of algae in halite endolithic communities are correlated to atmospheric moisture in the hyper-arid zone of the Atacama Desert. *Environ. Microbiol.* **17**, 299–315 (2015).
5. Crits-Christoph, A. *et al.* Functional interactions of archaea, bacteria and viruses in a hypersaline endolithic community. *Environ. Microbiol.* **18**, 2064–2077 (2016).
6. Finstad, K. M. *et al.* Microbial community structure and the persistence of cyanobacterial populations in salt crusts of the hyperarid Atacama Desert from genome-resolved metagenomics. *Front. Microbiol.* **8**, 1435 (2017).
7. Wierzchos, J., Ascaso, C. & McKay, C. P. Endolithic cyanobacteria in halite rocks from the hyperarid core of the Atacama Desert. *Astrobiology* **6**, 415–422 (2006).
8. Davila, A. F. *et al.* Facilitation of endolithic microbial survival in the hyperarid core of the Atacama Desert by mineral deliquescence. *J. Geophys. Res. Biogeosci.* **113**, 561 (2008).
9. Davila, A. F. *et al.* In situ metabolism in halite endolithic microbial communities of the hyperarid Atacama Desert. *Front. Microbiol.* **6**, 1035 (2015).
10. Uritskiy, G. *et al.* Halophilic microbial community compositional shift after a rare rainfall in the Atacama Desert. *ISME J.* **13**, 2737–2749 (2019).
11. Ziolkowski, L. A., Wierzchos, J., Davila, A. F. & Slater, G. F. Radiocarbon evidence of active endolithic microbial communities in the hyperarid core of the Atacama Desert. *Astrobiology* **13**, 607–616 (2013).
12. Colesie, C., Büdel, B. & Green, A. T. G. Endolithic communities in the McMurdo Dry Valleys: Biomass, turnover, cyanobacteria and location—A preliminary insight. *Algol. Stud.* **151–152**, 51–68 (2016).
13. Mergelov, N. *et al.* Alteration of rocks by endolithic organisms is one of the pathways for the beginning of soils on Earth. *Sci. Rep.* **8**, 1–15 (2018).
14. Uritskiy, G. *et al.* Environmental factors driving spatial heterogeneity in desert halophile microbial communities. *Front. Microbiol.* **11**, 2571 (2020).
15. Ríos, A. D. *et al.* Comparative analysis of the microbial communities inhabiting halite evaporites of the Atacama Desert. *Int. Microbiol.* **13**, 79–89 (2010).
16. Gunde-Cimerman, N., Plemenitaš, A. & Oren, A. Strategies of adaptation of microorganisms of the three domains of life to high salt concentrations. *FEMS Microbiol. Rev.* **42**, 353–375 (2018).
17. Rawls Katherine, S., Martin Jonathan, H. & Maupin-Furlow Julie, A. Activity and transcriptional regulation of bacterial protein-like glycerol-3-phosphate dehydrogenase of the haloarchaea in *Haloferax volcanii*. *J. Bacteriol.* **193**, 4469–4476 (2011).
18. Teichmann, L. *et al.* From substrate specificity to promiscuity: Hybrid ABC transporters for osmoprotectants. *Mol. Microbiol.* **104**, 761–780 (2017).
19. Chandra, G., Chater, K. F. & Bornemann, S. Unexpected and widespread connections between bacterial glycogen and trehalose metabolism. *Microbiology* **157**, 1565–1572 (2011).
20. Imhoff, J. F., Rahn, T., Künzel, S., Keller, A. & Neulinger, S. C. Osmotic adaptation and compatible solute biosynthesis of phototrophic bacteria as revealed from genome analyses. *Microorganisms* **9**, 46 (2020).
21. Uritskiy, G. *et al.* Cellular life from the three domains and viruses are transcriptionally active in a hypersaline desert community. *Environ. Microbiol.* **23**, 3401–3417 (2021).
22. Fernández, A. B., León, M. J., Vera, B., Sánchez-Porro, C. & Ventosa, A. Metagenomic sequence of prokaryotic microbiota from an intermediate-salinity pond of a saltern in Isla Cristina, Spain. *Genome. Annouc.* **2**, e00045 (2014).
23. Shu, W.-S. & Huang, L.-N. Microbial diversity in extreme environments. *Nat. Rev. Microbiol.* **20**, 219–235 (2022).
24. Bellas, C. M. & Sommaruga, R. Polinton-like viruses are abundant in aquatic ecosystems. *Microbiome* **9**, 13 (2021).
25. Potts, M. Desiccation tolerance of prokaryotes. *Microbiol. Rev.* **58**, 755–805 (1994).
26. Lebre, P. H., De Maayer, P. & Cowan, D. A. Xerotolerant bacteria: Surviving through a dry spell. *Nat. Rev. Microbiol.* **15**, 285–296 (2017).
27. Oren, A. Thermodynamic limits to microbial life at high salt concentrations. *Environ. Microbiol.* **13**, 1908–1923 (2011).
28. Kimbrel, J. A. *et al.* Microbial community structure and functional potential along a hypersaline gradient. *Front. Microbiol.* **9**, 1492 (2018).
29. Dillon, J., Carlin, M., Gutierrez, A., Nguyen, V. & McLain, N. Patterns of microbial diversity along a salinity gradient in the Guerrero Negro solar saltern, Baja CA Sur, Mexico. *Front. Microbiol.* **4**, 399 (2013).
30. Fernández, A. B. *et al.* Comparison of prokaryotic community structure from Mediterranean and Atlantic saltern concentrator ponds by a metagenomic approach. *Front. Microbiol.* **5**, 196 (2014).
31. Oren, A., Baxter, B. K. & Weimer, B. C. Microbial communities in salt lakes: Phylogenetic diversity, metabolic diversity, and in situ activities. *Nat. Resour. Environ. Iss.* **15**, 51 (2009).
32. Becker, E. A. *et al.* Phylogenetically driven sequencing of extremely halophilic archaea reveals strategies for static and dynamic osmo-response. *PLoS Genet.* **10**, e1004784 (2014).
33. Graziano, G. & Merlino, A. Molecular bases of protein halotolerance. *Biochim. Biophys. Acta. Proteins Proteom.* **1844**, 850–858 (2014).
34. Paul, S., Bag, S. K., Das, S., Harvill, E. T. & Dutta, C. Molecular signature of hypersaline adaptation: Insights from genome and proteome composition of halophilic prokaryotes. *Genome Biol.* **9**, 1–19 (2008).
35. Fernández, A. B. *et al.* Prokaryotic taxonomic and metabolic diversity of an intermediate salinity hypersaline habitat assessed by metagenomics. *FEMS Microbiol. Ecol.* **88**, 623–635 (2014).

36. Andrei, A. -Ş, Banciu, H. L. & Oren, A. Living with salt: Metabolic and phylogenetic diversity of archaea inhabiting saline ecosystems. *FEMS Microbiol. Lett.* **330**, 1–9 (2012).
37. Falb, M. *et al.* Metabolism of halophilic archaea. *Extremophiles* **12**, 177–196 (2008).
38. Oren, A. Glycerol metabolism in hypersaline environments. *Environ. Microbiol.* **19**, 851–863 (2017).
39. Sankaranarayanan, K., Lowenstein, T. K., Timofeeff, M. N., Schubert, B. A. & Lum, J. K. Characterization of ancient DNA supports long-term survival of Haloarchaea. *Astrobiology* **14**, 553–560 (2014).
40. Sankaranarayanan, K., Timofeeff, M. N., Spathis, R., Lowenstein, T. K. & Lum, J. K. Ancient microbes from halite fluid inclusions: Optimized surface sterilization and DNA extraction. *PLoS ONE* **6**, e20683 (2011).
41. Wood, S. N. Fast stable restricted maximum likelihood and marginal likelihood estimation of semiparametric generalized linear models. *J. R. Stat. Soc. Ser. B (Stat. Method.)* **73**, 3–36 (2011).
42. Wood, S. N., Pya, N. & Säfken, B. Smoothing parameter and model selection for general smooth models. *J. Am. Stat. Assoc.* **111**, 1548–1563 (2016).
43. Hoehler, T. M., Bains, W., Davila, A., Parenteau, M. & Pohorille, A. *Life's Requirements, Habitability, and Biological Potential* (University of Arizona Press Tucson, 2020).
44. Cáceres, L. *et al.* Relative humidity patterns and fog water precipitation in the Atacama Desert and biological implications. *J. Geophys. Res. Biogeosci.* **112**, 344 (2007).
45. Warren-Rhodes, K. A. *et al.* Hypolithic cyanobacteria, dry limit of photosynthesis, and microbial ecology in the hyperarid Atacama Desert. *Microb. Ecol.* **52**, 389–398 (2006).
46. Uritskiy, G. V., DiRuggiero, J. & Taylor, J. MetaWRAP—A flexible pipeline for genome-resolved metagenomic data analysis. *Microbiome* **6**, 1–13 (2018).
47 Li, D., Liu, C.-M., Luo, R., Sadakane, K. & Lam, T.-W. MEGAHIT: An ultra-fast single-node solution for large and complex metagenomics assembly via succinct de Bruijn graph. *Bioinformatics* **31**, 1674–1676 (2015).
48. Kang, D. D. *et al.* MetaBAT 2: An adaptive binning algorithm for robust and efficient genome reconstruction from metagenome assemblies. *PeerJ* **7**, e7359 (2019).
49. Nurk, S., Meleshko, D., Korobeynikov, A. & Pevzner, P. A. metaSPAdes: A new versatile metagenomic assembler. *Genome Res.* **27**, 824–834 (2017).
50. Olm, M. R., Brown, C. T., Brooks, B. & Banfield, J. F. dRep: A tool for fast and accurate genomic comparisons that enables improved genome recovery from metagenomes through dereplication. *ISME J.* **11**, 2864–2868 (2017).
51. Parks, D. H., Imelfort, M., Skennerton, C. T., Hugenholtz, P. & Tyson, G. W. CheckM: Assessing the quality of microbial genomes recovered from isolates, single cells, and metagenomes. *Genome Res.* **25**, 1043–1055 (2015).
52. Olm, M. R. *et al.* Consistent metagenome-derived metrics verify and delineate bacterial species boundaries. *Msystems* **5**, e00731 (2020).
53. Oksanen, J. *et al.* The vegan package. In *Community Ecology Package*, 631–637 (2007).
54. Paradis, E. & Schliep, K. ape 5.0: An environment for modern phylogenetics and evolutionary analyses in R. *Bioinformatics* **35**, 526–528 (2019).
55. Chen, I. M. A. *et al.* IMG/M v. 5.0: An integrated data management and comparative analysis system for microbial genomes and microbiomes. *Nucleic Acids Res.* **47**, D666–D677 (2019).
56. Hyatt, D. *et al.* Prodigal: Prokaryotic gene recognition and translation initiation site identification. *BMC Bioinform.* **11**, 1–11 (2010).
57. Wu, S. & Zhu, Y. ProPAS: Standalone software to analyze protein properties. *Bioinformation* **8**, 167–169 (2012).
58. Chaumeil, P.-A., Mussig, A. J., Hugenholtz, P. & Parks, D. H. GTDB-Tk: A toolkit to classify genomes with the Genome Taxonomy Database. *Bioinformatics* **36**, 1925–1927 (2020).
59. Parks, D. H. *et al.* A complete domain-to-species taxonomy for Bacteria and Archaea. *Nat. Biotechnol.* **38**, 1079–1086 (2020).
60. Lee, M. D. GToTree: A user-friendly workflow for phylogenomics. *Bioinformatics* **35**, 4162–4164 (2019).
61. Kanehisa, M., Sato, Y. & Morishima, K. BlastKOALA and GhostKOALA: KEGG tools for functional characterization of genome and metagenome sequences. *J. Mol. Biol.* **428**, 726–731 (2016).
62. Wong, H. L., MacLeod, F. I., White, R. A., Visscher, P. T. & Burns, B. P. Microbial dark matter filling the niche in hypersaline microbial mats. *Microbiome* **8**, 135 (2020).
63. Guo, J. *et al.* VirSorter2: A multi-classifier, expert-guided approach to detect diverse DNA and RNA viruses. *Microbiome* **9**, 1–13 (2021).
64. Nayfach, S. *et al.* CheckV assesses the quality and completeness of metagenome-assembled viral genomes. *Nat. Biotechnol.* **39**, 578–585 (2021).
65. Tisza, M. J., Belford, A. K., Dominguez-Huerta, G., Bolduc, B. & Buck, C. B. Cenote-Taker 2 democratizes virus discovery and sequence annotation. *Virus Evol.* **7**, 100 (2021).

Acknowledgements

This work was funded by NASA Grants 80NSSC19K0470 and NNX15AP18G. We thank the personnel at ALMA for their fieldwork support, hospitality, and access to the facility. The authors thank Peter R. McCullough and Dana Burton for fieldwork assistance. McCullough's travel was supported in part by the Space Telescope Science Institute's Director's Discretionary Fund under Grant D0001.82413. They thank Jacek Wierzchos for motivating this work via discussions and previous expeditions to the Atacama Desert.

Author contributions

J.D. and A.D. conceptualized and designed the study; J.D., A.D., C.P., and P.W. collected in-field samples; C.P. processed and sequenced samples; C.P. and J.D. analyzed the molecular data; A.D. and P.W. analyzed the climate data. All wrote the manuscript.

Competing interests

The authors declare no competing interests.

Additional information

Supplementary Information The online version contains supplementary material available at https://doi.org/10.1038/s41598-022-23437-w.

Correspondence and requests for materials should be addressed to J.D.